Brain Structure and Function (2019) 224:3171–3182
https://doi.org/10.1007/s00429-019-01952-3

ORIGINAL ARTICLE

The robust and independent nature of structural STS asymmetries

Jonathan S. Bain[2] · **Shir Filo**[1] · **Aviv A. Mezer**[1]

Received: 17 June 2019 / Accepted: 31 August 2019 / Published online: 13 September 2019

Abstract
The superior temporal sulcus (STS) is an important region for speech comprehension. The greater language network is known to exhibit asymmetries in both structure and function, and consistent with that theory are reports of STS structural asymmetry in MRI-based, morphological measures such as mean thickness and sulcal depth. However, it is not known how these individual STS structural asymmetries relate to each other, or how they interact with the broader language asymmetry that manifests in other brain regions. In this study, we assess the interrelations of STS asymmetries in the human brain in vivo, using four independent datasets to validate our findings. For morphological measurements, we identify STS laterality effects consistent between our datasets and with the literature: leftward for surface area, and rightward for sulcal depth and mean thickness. We then add two more measurements of STS asymmetry: in T1, a quantitative index of the tissue's underlying biophysical properties; and in the projections to the STS from the arcuate fasciculus, a left-lateralized white-matter bundle that connects temporal regions (including STS) with frontal regions (including Broca's area). For these two new measurements, we identify no effect for T1 and a leftward effect for arcuate projections. We then test for correlations between these STS asymmetries, and find associations mainly between measurements of the same type (e.g., two morphological measurements). Finally, we ask if STS asymmetry is preferentially related to Broca asymmetry, as these are both important language regions and connected via the arcuate fasciculus. Using a linear model with cross-validation, we find that random regions are as successful as Broca's area in predicting STS, and no indication of a hypothesized leftward asymmetry. We conclude that although these different STS asymmetries are robust across datasets, they are not trivially related to each other, suggesting different biological or imaging sources for different aspects of STS lateralities.

Keywords Arcuate fasciculus · Asymmetry · Broca's area · Language · Replication

Introduction

A key feature of the human brain is a lateralization for language (Hutsler and Galuske 2003; Toga and Thompson 2003; Vigneau et al. 2006). Language-related asymmetries in the brain were discovered in early clinical and postmortem work (Broca 1865; Geschwind and Levitsky 1968; Wernicke 1874), and their significance is supported by an absence or reduction of such asymmetries in animal models (Croxson et al. 2018; Leroy et al. 2015; Rilling 2014; Schenker et al. 2010). In humans, some of these lateralized regions have been proposed to participate in the classical model of language, whereby the white-matter bundle called the arcuate fasciculus connects inferior frontal and temporal cortical regions (Geschwind 1970; Hagoort 2014; Poeppel and Hickok 2004). In this work, we examine one of these temporal cortical regions, the superior temporal sulcus (STS), and assess how its structural asymmetries relate to the asymmetries of the broader language network.

The STS comprises the sulcus between the superior and middle temporal gyri, and is considered to be included in Wernicke's area (though the exact location of Wernicke's area is controversial—see DeWitt and Rauschecker 2013; Tremblay and Dick 2016). Through case reports, Wernicke

Electronic supplementary material The online version of this article (https://doi.org/10.1007/s00429-019-01952-3) contains supplementary material, which is available to authorized users.

✉ Jonathan S. Bain
jonathan.bain@mail.huji.ac.il

[1] The Edmond and Lily Safra Center for Brain Sciences, The Hebrew University of Jerusalem, Jerusalem, Israel

[2] The Edmond and Lily Safra Center for Brain Sciences, Goodman Building, Room 2202, The Hebrew University of Jerusalem, The Edmond J. Safra Campus at Givat Ram, 91904 Jerusalem, Israel

(1874) postulated that this temporal area was important for speech comprehension. This has been supported more recently using MRI (Hickok and Poeppel 2016), as the STS has been shown to participate in behaviors such as language comprehension (Dehaene et al. 1997; McGettigan et al. 2012) and voice identification (Bodin et al. 2018; Warren et al. 2006).

In these studies the STS shows activation in response to auditory language stimuli. Importantly, in most of these studies an asymmetrical effect is detected, which complements the structural asymmetries that have been reported in this region. Morphological measures such as surface area and cortical thickness have been shown to be right- and left-lateralized, respectively (Kong et al. 2018). The depth of the sulcus is usually deeper in the right hemisphere, while the left is more prone to irregular sulcal interruptions called *plis de passage* (Le Guen et al. 2018; Leroy et al. 2015).

In addition to the STS, other language-relevant regions are also known to exhibit laterality. In the inferior frontal gyrus, Broca's area exhibits asymmetry in MRI-based features like thickness (Kong et al. 2018) and functional activation (Keller et al. 2009; Rogalsky and Hickok 2010). Similar effects have been reported in Broca's area using postmortem analyses like cell staining (Amunts et al. 1999, 2003) and receptor profiles (Zilles and Amunts 2018; Zilles et al. 2015).

Broca's area is at one end of the arcuate fasciculus, while the other end reaches temporoparietal regions that include the STS (Rilling et al. 2012). The arcuate fasciculus is itself related to language (Catani et al. 2007; Meyer et al. 2012; Lopez-Barroso et al. 2013). Additionally, it too is known to be lateralized, as in vivo studies show a leftward asymmetry for arcuate volume (Bain et al. 2019; Nucifora et al. 2005; Thiebaut de Schotten et al. 2011) and microstructural properties (Beaulieu 2002; Jones et al. 2013; Lebois 2014).

Asymmetries in language-related gray-matter regions (like Broca's area) and in related white-matter pathways (like the arcuate fasciculus) have been documented independently. However, it is not known how STS asymmetry interacts with asymmetry measures in other parts of the classical network. In this work, we evaluate the laterality of the STS within the context of language lateralization. We examine whether different lateralized components (both within a region and between multiple regions) are interrelated under one broad framework for leftward language lateralization, or alternatively if they are independent. We start by evaluating the laterality of single STS measurements with multiple datasets, in an effort to replicate previous findings. We then test if laterality is correlated within a region, evaluating whether these individual STS measurements covary or are independent. Finally, we test if laterality is correlated between regions, using components of the classical model as a framework. We hypothesize that STS measurements can be better predicted by measurements in Broca's area, which is another language-relevant region, than by measurements in other, non-language regions. Furthermore, since Broca's area and the arcuate fasciculus each display a leftward laterality as consistent with language asymmetry, we hypothesize an increase in predictive power using the left regions than their right homologues. Together, the results of these analyses help illustrate the connected and independent components of the lateralized language network.

Methods

Datasets

The analysis was performed on four datasets. This was done both to increase the sample size and statistical power of our analysis, and to verify our results across independently collected data. All subjects have diffusion and anatomical data, which allow for most of our analyses, while the first two datasets also have quantitative data, which allow for an additional analysis using the calculated quantitative T1 maps.

Dataset 1 (D1)

The first dataset (D1) was taken from a larger dataset (Yeatman et al. 2014) collected at Stanford University (USA). We selected 33 adults (17 men, 16 women; mean age 33.55 ± 11.72 years, range 18–55 years).

D1 data were collected at Stanford University's Center for Cognitive and Neurobiological Imaging (http://www.cni.stanford.edu), using a 3T General Electric Discovery 750 (General Electric Healthcare, Milwaukee, WI, USA) equipped with a 32-channel head coil (Nova Medical, Wilmington, MA, USA). Data collection procedures were approved by the Stanford University Institutional Review Board. Subjects were recruited from the San Francisco area and were screened for neurological, cognitive and psychiatric disorders. All subjects provided informed consent.

The diffusion MRI (dMRI) data for each subject comprised a twice refocused spin-echo sequence (Reese et al. 2003) with full-brain coverage and yielded HARDI data. These scans included 96 noncollinear diffusion-weighted directions with a b value of 2000 s/mm^2, and eight non-diffusion-weighted images with a b value of 0 s/mm^2. The diffusion images had a resolution of $2 \times 2 \times 2$ mm^3, with a repetition time of 7800 ms and an echo time of 93.6 ms. The gradient strength was 53 mT/m and the slew rate was 200 mT/m/ms.

The quantitative MRI (qMRI) data for each subject comprised four high-resolution spoiled gradient echo (SPGR) scans and four low-resolution spin-echo inversion recovery (SEIR) scans (Mezer et al. 2013, 2016). The SPGR images

had a resolution of $1 \times 1 \times 1$ mm^3 and flip angles of 4°, 10°, 20° and 30°, with repetition time and echo time of 14 ms and 2.4 ms, respectively. The SEIR images, which were used to correct for the transmit-coil inhomogeneities, had a resolution of $2 \times 2 \times 4$ mm^3 and inversion times of 50 ms, 400 ms, 1200 ms and 2400 ms, with a repetition time of 3 ms and echo time set to "minimum full".

Dataset 2 (D2)

The second dataset (D2) was collected at The Hebrew University of Jerusalem (Israel). The subjects comprised 33 adults (21 men, 12 women; mean age 47.79 ± 20.97 years, range 24–77 years). D2 was taken from a dataset in Filo et al. (2019).

D2 data were collected at The Hebrew University's Edmond and Lily Safra Center (ELSC) for Brain Sciences' Neuroimaging Unit (https://elsc.huji.ac.il/enu/home), using a 3T Siemens Magnetom Skyra scanner equipped with a 32-channel head coil. Data collection procedures were approved by the Israeli Ministry of Health in accordance with the Declaration of Helsinki. All subjects provided informed consent.

The dMRI data for each subject comprised a diffusion-weighted spin-echo sequence with full-brain coverage and yielded HARDI data. These scans included 64 noncollinear diffusion-weighted directions with a b value of 2000 s/mm^2, and eight non-diffusion-weighted images with a b value of 0 s/mm^2. The diffusion images had a resolution of $1.5 \times 1.5 \times 1.5$ mm^3, with a repetition time of 6000 ms and an echo time of 95.8 ms. The gradient strength was 45 mT/m and the slew rate was 200 mT/m/ms.

Similar to D1, the qMRI data for D2 comprised four spoiled gradient echo scans and four spin-echo inversion recovery scans. We used a fast low-angle shot (FLASH) sequence, which is Siemens' equivalent of General Electric's SPGR. The FLASH images had a resolution of $1 \times 1 \times 1$ mm^3 and flip angles of 4°, 10°, 20° and 30°, with repetition time of 19 ms and five echo times equally spaced between 3.34 and 14.02 ms. The SEIR images had a resolution of $2 \times 2 \times 3$ mm^3 and inversion times of 200 ms, 400 ms, 1200 ms and 2400 ms, with a repetition time of 2920 ms and echo time of 49 ms.

Dataset 3 (D3)

The third dataset (D3) was also collected at the Hebrew University of Jerusalem (Israel), using the same hardware as for D2 (see also Bain et al. in preparation). The subjects comprised 28 adults (12 men, 16 women; mean age 25.50 ± 4.61 years, range 19–36 years). Data collection procedures were approved by the Israeli Ministry of Health in accordance with the Declaration of Helsinki. All subjects provided informed consent.

Compared to D2, the acquisition parameters for D3 diffusion sequence differed in the following ways: the voxel size was $1.7 \times 1.7 \times 1.7$ mm^3, the repetition time was 4000 ms and the echo time was 96.2 ms.

Dataset 4 (D4)

The fourth dataset (D4) was downloaded from the publicly available Human Connectome Project (Van Essen et al. 2013). We selected the data subset consisting of 100 unrelated subjects (46 men, 54 women; 17 subjects aged 22–25, 40 subjects aged 26–30, 42 subjects aged 31–35, 1 subject aged 36+).

We downloaded the HCP100 data that already had been passed through the HCP preprocessing pipeline (Glasser et al. 2013). For each subject, the data included a T1-weighted image with resolution of $0.7 \times 0.7 \times 0.7$ mm^3. The dMRI data consisted of 90 noncollinear diffusion-weighted directions with a b value of 2000 s/mm^2, and six non-diffusion-weighted images with a b value of 0 s/mm^2. The diffusion images had a resolution of $1.25 \times 1.25 \times 1.25$ mm^3.

Volumetric analysis

For each subject in all four datasets, we used the T1-weighted image to derive a whole-brain parcellation in subject space using the recon-all function in FreeSurfer (version 5.3.0, http://surfer.nmr.mgh.harvard.edu/). The output files include cortical surfaces that allow for the calculation of four volumetric measurements: surface area, gray volume and mean thickness, as well as sulcal depth from the .sulc displacement file. Additionally, FreeSurfer parcellates the brain according the Desikan atlas (Desikan et al. 2006) using gyrification landmarks, which allows us to identify the STS as well as 37 other cortical regions. For each cortical region in the Desikan atlas we created a surface at the midpoint of its gray matter, and used the FreeSurfer function mris_anatomical_stats to calculate the mean value of each measurement for that region's midpoint surface.

Diffusion analysis

For each subject in all four datasets, we used the Vistasoft (http://github.com/vistalab/vistasoft/mrDiffusion) and MRtrix (version 0.2.12, https://www.nitrc.org/projects/mrtrix/) software packages for preprocessing, which included corrections for subject motion and eddy currents.

To identify the arcuate fasciculus, we first computed a tractogram of streamlines covering the whole brain. We used a probabilistic tractography algorithm on a

constrained spherical deconvolution (CSD) model of the data (Tournier et al. 2007). We used MRtrix3 (https://github.com/MRtrix3/mrtrix3) with a maximum harmonic order (l_{max}) of 8 to fit a multi-lobe shape to represent the fiber orientation distribution in each voxel, and then to generate 500,000 streamlines using the iFOD2 method (Tournier et al. 2010). Streamlines were seeded at the gray matter–white matter boundary, as determined via anatomically constrained tractography (Smith et al. 2012).

We further evaluated the resultant tractogram by using LiFE, a tractography-evaluation method (Pestilli et al. 2014; https://github.com/francopestilli/life). In this global method, a set of streamlines is reduced by assigning each streamline a weight that corresponds to its contribution to predicting the original diffusion data. We apply these weights to the tractogram by first discarding any streamline with a zero weight, and then by including multiple copies of each remaining streamline, where the number of copies for each streamline is its weight divided by the smallest weight and rounded. In this way, nonpredictive streamlines are eliminated while strongly predictive streamlines are given more emphasis in the tractogram.

In order to extract the arcuate fasciculus from this LiFE-weighted tractogram, we used Matlab (version 9.3.0, R2017b) to run the software package Automated Fiber Quantification (AFQ; Yeatman et al. 2012; https://github.com/yeatmanlab/AFQ). AFQ extracts the left and right arcuate from tractogram by using the Mori atlas (Wakana et al. 2007), which defines 20 known major white-matter tracts through the use of white-matter waypoint region-of-interest planes. For the arcuate, a streamline is included if it passes through the two arcuate-defining planes (one axial and one coronal) in its respective hemisphere. Before returning a final arcuate bundle, AFQ's cleaning procedure first removes outlier streamlines, defined as five standard deviations away from the fiber tract core or four standard deviations above the mean streamline length.

Quantitative T1 analysis

For the D1 and D2 datasets, we used the SEIR images and either the SPGR (for D1) or FLASH (for D2) images to compute a quantitative T1 map, following Mezer et al. (2013). To calculate the T1 map, we used the mrQ software (version 2.0, https://github.com/mezera/mrQ). First, mrQ calls ANTs (version 2.1.0; Avants et al. 2011) to align the SPGR/FLASH and SEIR images, and then calculates the transmit-coil inhomogeneities. Then the T1 map is fitted using a weighted linear least squares fitting algorithm (Chang et al. 2008).

Cross-validation analysis

Our first analyses using this data were to quantify lateralities for different measurements within the STS. We also used the data to relate STS measurements to those of other cortical regions. We hypothesized that STS measurements would exhibit a preferential relationship with those of Broca's area, compared to those of other non-language regions. We also hypothesized a stronger relationship for the left hemisphere than for the right. To test this, we used a linear model to predict STS measurements, using the measurements from either the three components of Broca's area (pars opercularis, pars triangularis, pars orbitalis) or three other regions (postcentral gyrus, lateral occipital region and anterior medial temporal gyrus) which are not specifically language-related and not known to be functionally related to the STS (Margulies et al. 2016; Yeo et al. 2011). We used a cross-validation approach pooling all four datasets, training on 75% of subjects and running 2000 iterations.

Results

Relating measures of STS asymmetry

The STS is a key part of the language network, and is known to exhibit lateralization in both function and structure. Commonly measured structural asymmetries in the STS include gray-matter properties derived from surface-based measurements, such as mean thickness; less is known about STS asymmetry for quantitative gray-matter measures such as T1, or about the white-matter asymmetry of the arcuate fasciculus projecting to the STS. Here, we measure and validate these lateralities, and describe their interrelations, in four independent datasets.

In Fig. 1 we illustrate STS laterality for six measurements, using a two-tailed, paired-sample t test with $\alpha = 0.05$ (Bonferroni-corrected) to test for asymmetry (see also Table 1). For the surface-based measurements, we identify a rightward laterality effect that is consistent across all four datasets for both thickness (Fig. 1a) and sulcal depth (Fig. 1b), and a leftward laterality for three datasets for surface area (Fig. 1d). These results are consistent with the literature (Kong et al. 2018; Leroy et al. 2015). Importantly, those studies detect laterality effects separately for different datasets. Here, we evaluate STS laterality for multiple measures concurrently across the same subjects.

We complement these volume- and surface-based measurements with two other measures of STS laterality. First, we test for STS asymmetry in T1, a quantitative measure that reflects the underlying biophysical nature of the tissue. For this analysis we used a subset of the data, as only D1 and D2 include quantitative T1 data (see "Methods"—"Datasets").

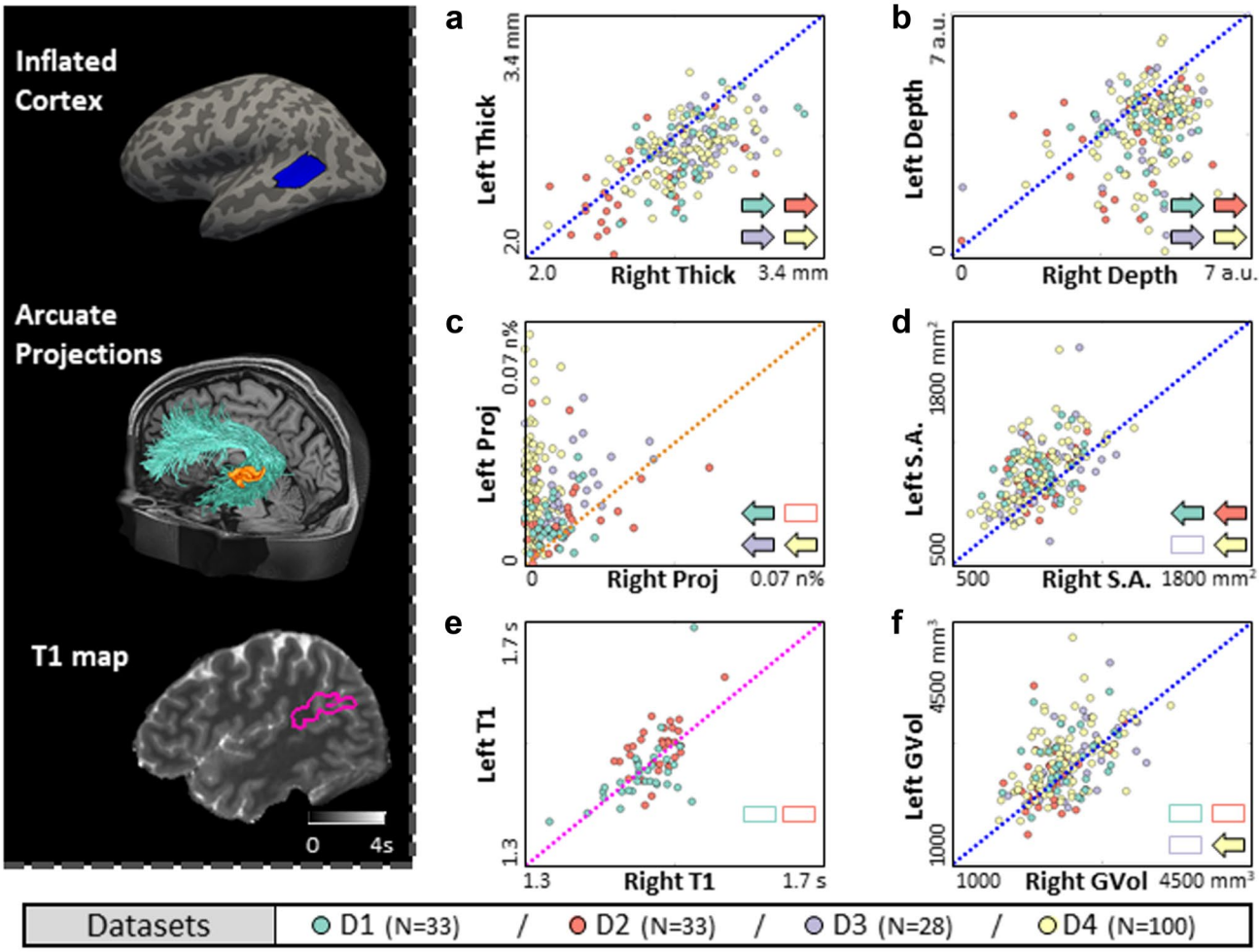

Fig. 1 Evaluating laterality in the superior temporal sulcus (STS) in six measurements across four datasets (D1–D4). Left inset: sample subject's left STS, illustrated in blue on the FreeSurfer inflated cortex (top); in orange alongside the cyan arcuate fasciculus streamlines (middle); and in a magenta outline atop the T1 map (bottom). Right: **a**–**f** show individual subjects' left and right values for six measurements, with the identity lines' color matching the inset. The filled arrows in the bottom-right of each panel indicate the direction for which a statistically significant effect (adjusted for multiple comparisons) was detected for that dataset, while an unfilled rectangle indicates that no statistically significant effect could be detected (see Table 1). The color of the datapoints and arrows/rectangles correspond to the four datasets (green, D1; red, D2; purple, D3; yellow, D4). All four datasets showed a statistically significant rightward laterality for mean thickness (Thick, **a**) and sulcal depth (Depth, **b**), while three datasets showed a statistically significant leftward laterality for arcuate projections (Proj, **c**) and surface area (S.A., **d**). For quantitative T1 values (T1, **e**) we detected no significant laterality in either of the two datasets for which we had quantitative T1 maps, while only D4 showed a significant laterality for gray volume (GVol, **f**). *a.u.* arbitrary units, *n%* percent of arcuate streamlines normalized by size of STS surface area

We identify no significant T1 laterality for either dataset (Fig. 1e).

For a second additional test of STS asymmetry, we expand our view to include the white-matter pathways that project to STS. In a previous work (Bain et al. 2019), we show the leftward laterality for streamline count of the arcuate fasciculus. Here, we analyze a specific subset of those streamlines, namely, those that project to the STS in each hemisphere. In our analysis, we control for the existing hemispheric asymmetries both in the number of total arcuate streamlines as well as in the surface area of the STS (see Fig. A1). We detect a statistically significant leftward asymmetry for three datasets (Fig. 1c), suggesting a relevant white-matter asymmetry concurrent with the gray-matter asymmetry as described above.

In assessing our projection asymmetry results, we observe the strongest asymmetry for dataset D4, with a comparatively smaller set of values for projections to the right hemisphere. Since D4 had the finest dMRI resolution of our four datasets, we downsampled the diffusion data of 40 D4 subjects from 1.25 to 2 mm^3 to test the effect of resolution on these results. We found that downsampling

Table 1 Measures of asymmetry in the superior temporal sulcus (STS) for six measures across four datasets (D1–D4)

Measure	Dataset	Right		Left		*t* stat	*p* value
		Mean	Std	Mean	Std		
Thick (mm)	D1	2.771	0.191	2.613	0.217	4.534	**7.65E−05**
	D2	2.568	0.253	2.422	0.201	3.993	**3.57E−04**
	D3	2.839	0.144	2.672	0.124	6.508	**2.52E−07**
	D4	2.742	0.172	2.617	0.155	7.776	**7.22E−12**
Depth (a.u.)	D1	4.557	0.720	3.446	1.080	4.800	**3.55E−05**
	D2	4.158	1.222	3.455	1.299	2.989	**5.35E−03**
	D3	4.681	1.044	3.588	1.361	3.854	**5.28E−04**
	D4	4.697	0.749	3.721	1.127	8.076	**1.65E−12**
AF Proj (*n*%)	D1	0.0065	0.0041	0.0123	0.0066	−4.694	**5.52E−05**
	D2	0.0090	0.0091	0.0143	0.0105	−2.554	1.56E−02
	D3	0.0110	0.0071	0.0225	0.0104	−5.920	**2.61E−06**
	D4	0.0023	0.0022	0.0223	0.0133	−14.792	**8.13E−27**
S.A. (mm^2)	D1	881.5	115.5	997.0	120.9	−4.773	**3.84E−05**
	D2	876.5	97.8	944.8	114.0	−3.218	**2.96E−03**
	D3	918.5	133.6	989.0	196.0	−2.346	2.53E−02
	D4	877.8	132.2	990.1	162.6	−7.926	**3.46E−12**
T1 (s)	D1	1.457	0.041	1.450	0.054	0.810	4.24E−01
	D2	1.477	0.030	1.490	0.040	−2.183	3.65E−02
GVol (mm^3)	D1	2,333.9	330.7	2,489.5	416.5	−1.992	5.50E−02
	D2	2,153.2	289.7	2,229.8	421.5	−1.022	3.15E−01
	D3	2,487.4	369.1	2,564.6	471.0	−1.035	3.08E−01
	D4	2,292.5	369.5	2,500.5	455.8	−5.040	**2.10E−06**

We used a two-tailed, paired-sample *t* test with $\alpha = 0.05$ (Bonferroni-corrected) to test for laterality in STS. Positive *t* stat values indicate a rightward laterality, while negative values indicate a leftward laterality. Significant *p* values marked in bold

Std standard deviation, *n%* percent of arcuate streamlines normalized by size of STS surface area, *a.u.* arbitrary units, *GVol* gray volume, *S.A.* surface area, *Thick* cortical thickness, *Proj* arcuate projections to STS, *Depth* sulcal depth, *T1* quantitative T1. See also Fig. A3–4

did not change the laterality of the result but did decrease its magnitude, making it more similar to the results with our other datasets (Fig. A2).

After quantifying the asymmetry for each of these measures separately, we tested whether these measures were correlated with each other. In Fig. 2 we show the correlation

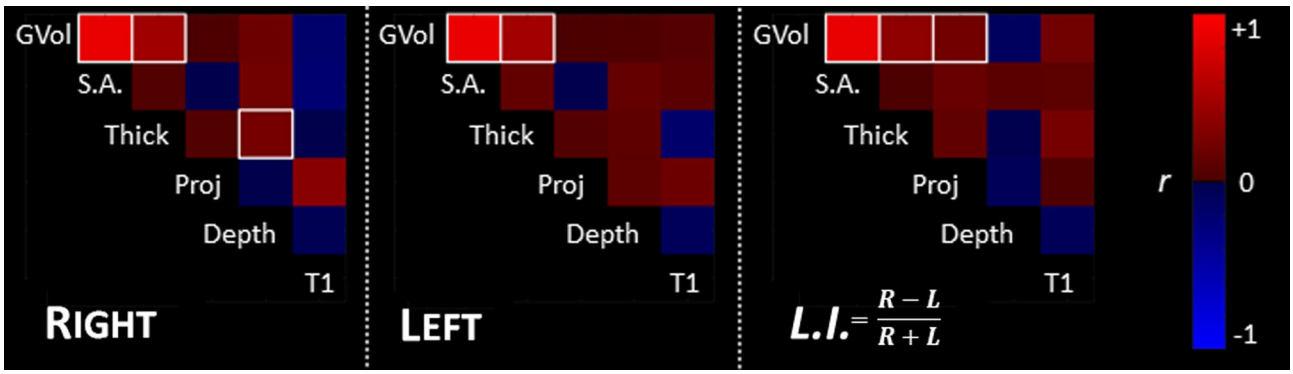

Fig. 2 Upper triangular of the correlation matrix for the six measurements of the superior temporal sulcus (STS). We calculated the correlation matrix separately for the right and left STS, as well for the STS laterality index (L.I.), defined as (right minus left) ÷ (right plus left), where a positive L.I. indicates a rightward laterality and a negative L.I. a leftward laterality. Significant correlations marked by a white outline. See also Table 2 and Figs. A3–4. *GVol* gray volume, *S.A.* surface area, *Thick* cortical thickness, *Proj* arcuate projections to STS, *Depth* sulcal depth, *T1* quantitative T1

matrices for the six measures for the right and left STS independently, as well as for the STS's laterality index (L.I.), defined as (right minus left) ÷ (right plus left), where a positive L.I. indicates a rightward laterality and a negative L.I. a leftward laterality (see also Table 2). In Fig. A3 we show the correlation matrices for each dataset separately, and in Fig. A4 we show scatterplots for all subjects for the statistically significant pairings (corrected for multiple comparisons).

For all three of the right STS, left STS and STS L.I., we identify statistically significant positive correlations between the gray volume and surface area, as well as between the gray volume and thickness. We rationalize this result by the fact that these three measurements are interrelated, as they are derived from the same source (T1-weighted image). For the right hemisphere, we also identified a positive, statistically significant correlation between sulcal depth and mean thickness. For the subset of subjects with T1 maps, we identified no significant correlations between T1 values and any other morphological measure of the STS.

Next, we tested whether these STS measures of cortical gray matter were related to the percentage of white-matter projections of the arcuate fasciculus to the STS. We detect

Table 2 Correlations between pairs of the six different measurements of STS

			Measurement 1									
	GVol		**S.A.**		**Thick**		**Proj**		**Depth**		**T1**	
df (N-1)	193		193		193		193		193		65	
			r	***p***	***r***	***p***	***r***	***p***	***r***	***p***	***r***	***p***
Measurement 2	**GVol**	Right	**0.878**	**1.21E-62**	**0.465**	**1.02E-11**	0.021	7.71E-01	0.188	8.95E-03	-0.175	1.66E-01
		Left	**0.897**	**3.13E-69**	**0.483**	**1.23E-12**	0.013	8.58E-01	0.021	7.72E-01	0.057	6.54E-01
		L.I.	**0.877**	**2.09E-62**	**0.369**	**1.36E-07**	**0.222**	**2.00E-03**	-0.107	1.41E-01	0.211	9.35E-02
	--	--	**S.A.**	Right	0.043	5.55E-01	-0.007	9.27E-01	0.208	3.78E-03	-0.208	9.90E-02
	--	--		Left	0.129	7.43E-02	-0.020	7.85E-01	0.138	5.64E-02	0.085	5.03E-01
	--	--		L.I.	0.002	9.73E-01	0.162	2.50E-02	0.083	2.52E-01	0.104	4.11E-01
	--	--	--	--	**Thick**	Right	0.039	5.89E-01	**0.240**	**7.89E-04**	-0.013	9.19E-01
	--	--	--	--		Left	0.048	5.04E-01	0.109	1.33E-01	-0.165	1.94E-01
	--	--	--	--		L.I.	0.122	9.05E-02	-0.016	8.25E-01	0.238	5.82E-02
	--	--	--	--	--	--	**Proj**	Right	-0.004	9.57E-01	0.336	6.64E-03
	--	--	--	--	--	--		Left	0.095	1.89E-01	0.188	1.36E-01
	--	--	--	--	--	--		L.I.	-0.072	3.19E-01	0.021	8.71E-01
	--	--	--	--	--	--	--	--	**Depth**	Right	-0.050	6.96E-01
	--	--	--	--	--	--	--	--		Left	-0.079	5.37E-01
	--	--	--	--	--	--	--	--		L.I.	-0.074	5.60E-01

We list the *r* value and *p* value for the right STS, left STS, and the STS laterality index (L.I.), where L.I. = (right minus left) ÷ (right plus left). Significant correlations ($\alpha = 0.05$, Bonferroni-corrected) are marked in bold. Degrees of freedom (df) for the correlations of T1 with any other measurement is 65, as only datasets D1 and D2 have quantitative data, and only these datasets were used in these calculations; for other correlations, all four datasets were used ($df = 193$)

GVol gray volume, *S.A.* surface area, *Thick* cortical thickness, *Proj* arcuate projections to STS, *Depth* sulcal depth, *T1* quantitative T1. See also Fig. A3–4

positive, statistically significant correlations between the L.I.s of arcuate projections and gray volume, but no effect for the right or left hemispheres separately. Additionally, while a significant effect was detected for the four datasets pooled together, no dataset exhibited a significant effect individually.

Predicting STS asymmetry from distal regions

We replicated STS laterality for different measurements and identified correlations between them. Importantly, since we detected a relationship between the STS's morphological measures and the arcuate fasciculus's white-matter projections to it, we then asked whether measures in the STS were preferentially related to those in Broca's area, at the other end of the arcuate fasciculus. Using a linear model with cross-validation on the combined subjects in all four datasets, we predicted STS measurements from either Broca's area or other, non-arcuate-projecting areas. In Fig. 3 and Table 3 we show the result for mean thickness, while other measurements are shown in Fig. A5–7 and Table A1.

We were moderately successful in predicting STS thickness using the thickness of the three components of Broca's area ($R^2 = 0.279$ for the right STS and $R^2 = 0.378$ for the left), and did identify a stronger effect for the left hemisphere. However, the prediction was more successful using three non-language, non-contiguous regions ($R^2 = 0.328$ for the right STS and $R^2 = 0.417$ for the left). We also modeled each dataset separately, and while we find some variability between datasets, overall the results were similar to the model using all datasets combined. In total, these analyses suggest that there is large-scale morphological association between STS and other regions within the same hemisphere, yet this is not specific to Broca's area, at the other end of the

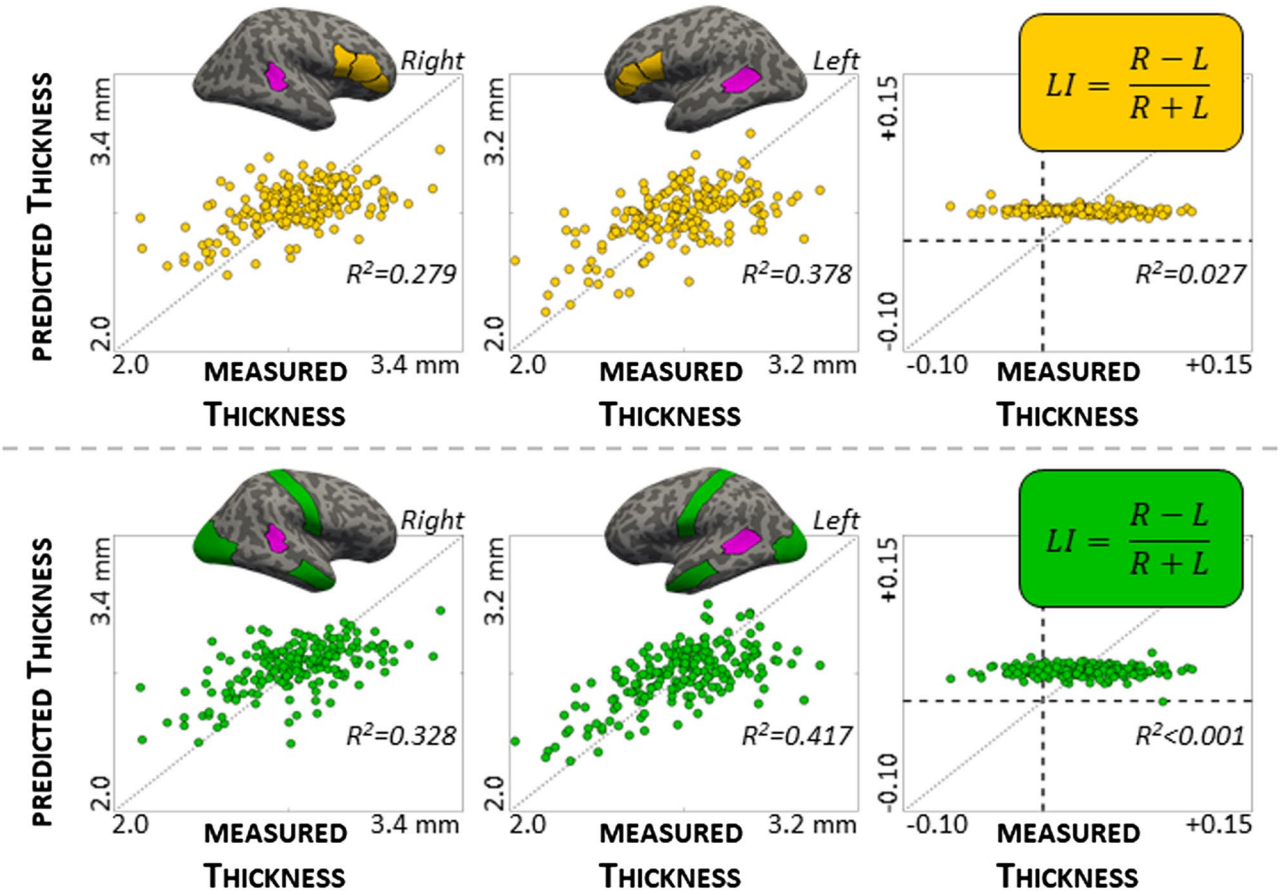

Fig. 3 Predicting mean thickness of the superior temporal sulcus (STS) from three distal areas. We used cross-validation on a linear model to predict the thickness of the STS (magenta on the inflated brains), using as predictors either three inferior frontal region (top row, yellow on the inflated brains) or three noncontiguous, non-language regions (bottom row, green on the inflated brains). Each point represents a single subject, averaged over all iterations where that subject was among the 25% test subjects. For both predictor sets, predicting the right STS (first column) was less successful than predicting the left STS (middle column), as expressed by the R^2 values. When we tried to predict the STS laterality index [L.I. = (right minus left) ÷ (right plus left)], we found a very flat relationship. Using the non-language regions were more successful than IFG regions for predicting STS thickness, suggesting an absence of arcuate- or language-specific preference linking STS and inferior frontal language areas. See also Table 3 and Figs. A5–7

Table 3 The relationship (r, p and R^2) between measured and predicted values for cortical thickness in the superior temporal sulcus (STS), as expressed graphically in Fig. 3

Measurement	Predictors	Hemisphere	r	p	R^2
Thickness ($N=194$)	IFG	Right	0.528	2.44E−15	0.279
		Left	0.614	1.60E−21	0.378
		L.I.	−0.165	2.15E−02	0.027
	Random	Right	0.573	2.71E−19	0.328
		Left	0.645	3.01E−24	0.417
		L.I.	−0.007	9.25E−01	<0.001

Values compare three regions in the inferior frontal gyrus (IFG) and three random regions, using the right hemisphere, left hemisphere, and the laterality index (L.I.), where L.I. = (right minus left) ÷ (right plus left). See also Table A1

arcuate fasciculus. Interestingly, while we could predict the subject difference in each hemisphere, we could not predict the laterality differences.

Discussion

In this work, we examine structural properties of the STS, a key component for language behavior, by evaluating its asymmetries across multiple measurements and multiple datasets. We validate known findings by detecting asymmetries in morphological measures, such as surface area and cortical thickness (Fig. 1), and complement these findings by adding two new measurements: the quantitative T1 of the gray matter, and the density of the white-matter projections of the arcuate fasciculus to the STS. We then test whether these different asymmetries were correlated with each other (Fig. 2), and find strong correlations only between measurements derived from the same source (e.g., gray volume and surface area). Finally, we hypothesized that measurements in the STS could be predicted by measurements in fellow language-related areas in the inferior frontal gyrus, but find no preferential specificity for these areas over control areas (Fig. 3). Additionally, predicting STS asymmetry is much less successful than predicting each hemisphere's volumetric measurements independently.

One important contribution of this work is the replication of these effects across four independent datasets. These datasets vary by factors such as dMRI resolution, scanner type and age range, but we detect commonalities across them all. An additional benefit of this work is showing all measurements concurrently: Kong et al. (2018) show surface area asymmetry and Leroy et al. (2015) show a sulcal depth asymmetry, and here we show both for the same subjects at the same time. This kind of replication, for both independent datasets and for different measurements concurrently, is especially important for in vivo MRI studies for which there is no reliable and verifiable gold standard (Cercignani et al. 2018; Daducci et al. 2016).

Of the six STS measurements we test, two show a leftward laterality (surface area and arcuate projections), two show a rightward laterality (cortical thickness and sulcal depth), and two show no laterality (gray volume and T1). While the morphological results are all consistent with previous findings (Le Guen et al. 2018; Kong et al. 2018), it is interesting to consider the presence of rightward asymmetries within the general framework of a leftward language laterality (Hutsler and Galuske 2003; Toga and Thompson 2003; Vigneau et al. 2006). The left STS has more sulcal interruptions (called *plis de passage*) than does the right, and STS is unique in that its *plis de passage* are both lateralized and heritable (Le Guen et al. 2018). *Plis de passage* may be attributable to different factors, such as white matter impacting the cortical surface (Hilgetag and Barbas 2006) or differences in cell layering (Hutsler 2003). This could cause the detection of greater thickness in the right STS than in the comparably more interrupted left. The rightward depth asymmetry might instead be reframed as a leftward interruption asymmetry; this would fit with the association of leftward asymmetry with language.

In accordance with this notion, we do detect a significant relationship between sulcal depth and cortical thickness for the right STS only (Fig. 2). However, when we compare the different asymmetries with each other, we mostly detect significant correlations between measurements that are derived from the same data type. This suggests that there may be several different and independent biological or imaging sources that contribute to the laterality of the STS and of the language system. Here we find reliable asymmetry effects with morphological measures such as cortical thickness and sulcal depth, and reliable asymmetry effects with diffusion measures such as projection asymmetry of the arcuate fasciculus, but these do not seem to relate to each other. This result may be attributable to the coarser resolution of the diffusion data; future work with higher resolution dMRI images could help reconcile these differences (Setsompop et al. 2018; Vu et al. 2015).

A third source may be captured by the quantitative T1 maps, which can reflect the biophysical contribution of underlying tissue components such as myelin (Stuber et al. 2014). In this work, quantitative data were available for only two of the four datasets, and we find no significant T1 asymmetry in the STS. This is in contrast with the arcuate fasciculus, the white-matter bundle that projects to STS and which exhibits a consistent leftward laterality for the quantitative T1 and even for the semi-quantitative T1-weighted to T2-weighted ratio (Bain et al. 2019). In order to determine how T1 relates to morphological- and diffusion-based measures, future research will require a larger sample of subjects with quantitative data, and probably also a higher resolution (Carey et al. 2018; Waehnert et al. 2016).

One source of STS laterality that is unavailable at the MRI level is in the neuroreceptor profiles. In a postmortem work, Zilles et al. (2015) show different profiles for the left and right STS. Interestingly, they find that the left STS profile is more similar to that in left Broca's area, while the right STS profile is more similar to that in neighboring parietal regions. This suggests a preferential hemispheric association, which might be expected from the classical model of language. In this work we used this asymmetry as an anatomical prior, hypothesizing that MRI-based measures of the left STS are more related to those in left inferior frontal gyrus than to those in other brain regions, or more than their right hemisphere counterparts. We did not find this to be the case, as our predictions of STS laterality were mostly flat and were as good using non-Broca predictors. In contrast to our observations, fMRI studies find activation of both these regions in language paradigms (Rampinini et al. 2017; Schell et al. 2017; Weber et al. 2016), suggesting that structural and functional laterality in the language network may not always be coupled.

The results from this analysis also serve to emphasize the importance of falsifiability when designing scientific experiments. We found that we can moderately predict the cortical thickness of the left STS using the left Broca's area, which would seem to support the notion of an interrelated left-hemisphere network within language-specific regions. However, in science one's aim should not be to support a hypothesis but to disprove the null hypothesis (Popper 1962; Wilkinson 2013): Here we find that the left Broca is as predictive as the right (disproving the claim of a preferential relationship with the left hemisphere) and that Broca's area is as predictive as a set of control regions (disproving the claim of a preferential relationship with the inferior frontal gyrus).

Conclusion

We report the structural asymmetries of the STS in vivo. We describe asymmetries that are consistent across four independent datasets, and suggest that these asymmetries may derive from different biophysical sources in the brain. Nevertheless, we find that STS structural asymmetry is not preferentially associated with asymmetry in Broca's area. Together we provide additional insight and validation for understanding the STS asymmetries.

Acknowledgements The authors thank B. Wandell for data collection, which was supported by the Weston Havens foundation, the National Science Foundation (BCS1228397) and National Institutes of Health (EY015000); Y. Grodzinsky and G. Agmon for additional data collection; and A. Erramuzpe and R. Schurr for their constructive comments and suggestions.

Author contributions SF collected data; JSB and AAM performed analysis and wrote the manuscript.

Funding This work was supported by the United States–Israel Binational Science Foundation (BCS1551330 to AAM); the Israel Science Foundation (0399306 to AAM).

Compliance with ethical standards

Conflict of interest The authors have no conflicts of interest to declare.

Research involving human participants and/or animals All procedures performed in studies involving human participants were in accordance with the ethical standards of the institutional and/or national research committee and with the 1964 Helsinki declaration and its later amendments or comparable ethical standards. This article does not contain any studies with animals performed by any of the authors.

Informed consent Informed consent was obtained from all individual participants included in the study.

References

Amunts K, Schleicher A, Burgel U, Mohlberg H, Uylings HB, Zilles K (1999) Broca's region revisited: cytoarchitecture and intersubject variability. J Comp Neurol 412(2):319–341

Amunts K, Schleicher A, Ditterich A, Zilles K (2003) Broca's region: cytoarchitectonic asymmetry and developmental changes. J Comp Neurol 465(1):72–89. https://doi.org/10.1002/cne.10829

Avants BB, Tustison NJ, Song G, Cook PA, Klein A, Gee JC (2011) A reproducible evaluation of ANTs similarity metric performance in brain image registration. NeuroImage 54(3):2033–2044. https://doi.org/10.1016/j.neuroimage.2010.09.025

Bain JS, Yeatman JD, Schurr R, Rokem A, Mezer AA (2019) Evaluating arcuate fasciculus laterality measurements across dataset and tractography pipelines. Hum Brain Mapp 40(13):3695–3711. https://doi.org/10.1002/hbm.24626

Beaulieu C (2002) The basis of anisotropic water diffusion in the nervous system—a technical review. NMR Biomed 15(7–8):435–455. https://doi.org/10.1002/nbm.782

Bodin C, Takerkart S, Belin P, Coulon O (2018) Anatomo-functional correspondence in the superior temporal sulcus. Brain Struct Funct 223(1):221–232. https://doi.org/10.1007/s00429-017-1483-2

Broca P (1865) Sur Le Siège de La Faculté Du Langage Articulé. Bulletins de La Société d'anthropologie de Paris 1(6):377–393. https://doi.org/10.3406/bmsap.1865.9495

Carey D, Caprini F, Allen M, Lutti A, Weiskopf N, Rees G, Callaghan MF, Dick F (2018) Quantitative MRI provides markers of intra-, inter-regional, and age-related differences in young adult cortical microstructure. NeuroImage 182(15):429–440. https://doi.org/10.1016/j.neuroimage.2017.11.066

Catani M, Allin MPG, Husain M, Pugliese L, Mesulam MM, Murray RM, Jones DK (2007) Symmetries in human brain language pathways correlate with verbal recall. Proc Natl Acad Sci USA 104(43):17163–17168. https://doi.org/10.1073/pnas.0702116104

Cercignani M, D NG, Tofts Paul (eds) (2018) Quantitative MRI of the brain: principles of physical measurement, 2nd edn. CRC Press, London

Chang L-C, Koay CG, Basser PJ, Pierpaoli C (2008) Linear least-squares method for unbiased estimation of T1 from SPGR signals. Magn Reson Med 60(2):496–501. https://doi.org/10.1002/mrm.21669

Croxson PL, Forkel SJ, Cerliani L, de Schotten MT (2018) Structural variability across the primate brain: a cross-species comparison. Cereb Cortex 28(11):1–13. https://doi.org/10.1093/cercor/bhx244

Daducci A, Dal Palú A, Descoteaux M, Thiran J-P (2016) Microstructure informed tractography: pitfalls and open challenges. Front Neurosci. https://doi.org/10.3389/fnins.2016.00247

Dehaene S, Dupoux E, Mehler J, Cohen L, Paulesu E, Perani D, van de Moortele PF, Lehéricy S, Le Bihan D (1997) Anatomical variability in the cortical representation of first and second language. NeuroReport 8(17):3809–3815

Desikan RS, Ségonne F, Fischl B, Quinn BT, Dickerson BC, Blacker D, Buckner RL et al (2006) An automated labeling system for subdividing the human cerebral cortex on MRI scans into gyral based regions of interest. NeuroImage 31(3):968–980. https://doi.org/10.1016/j.neuroimage.2006.01.021

DeWitt I, Rauschecker JP (2013) Wernicke's area revisited: parallel streams and word processing. Brain Lang 127(2):181–191. https://doi.org/10.1016/j.bandl.2013.09.014

Filo S, Shtangel O, Salamon N, Kol A, Weisinger B, Shifman S, Mezer AA (2019) Disentangling molecular alterations from water-content changes in the aging human brain using quantitative MRI. Nat Commun 10(1):3403

Geschwind N (1970) The organization of language and the brain. Science 170(3961):940–944

Geschwind N, Levitsky W (1968) Human brain: left–right asymmetries in temporal speech region. Science 161(3837):186–187. https://doi.org/10.1126/science.161.3837.186

Glasser MF, Sotiropoulos SN, Wilson JA, Coalson TS, Fischl B, Andersson JL, Xu J et al (2013) The minimal preprocessing pipelines for the Human Connectome Project. NeuroImage 80(Suppl C):105–124. https://doi.org/10.1016/j.neuroimage.2013.04.127

Hagoort P (2014) Nodes and networks in the neural architecture for language: Broca's region and beyond. Curr Opin Neurobiol 28:136–141. https://doi.org/10.1016/j.conb.2014.07.013

Hickok G, Poeppel D (2016) Neural basis of speech perception, Chapter 25. In: Hickok G, Small SL (eds) Neurobiology of language. Academic Press, San Diego, pp 299–310. https://doi.org/10.1016/B978-0-12-407794-2.00025-0

Hilgetag CC, Barbas H (2006) Role of mechanical factors in the morphology of the primate cerebral cortex. PLoS Comput Biol 2(3):e22. https://doi.org/10.1371/journal.pcbi.0020022

Hutsler JJ (2003) The specialized structure of human language cortex: pyramidal cell size asymmetries within auditory and language-associated regions of the temporal lobes. Brain Lang Underst Lang 86(2):226–242. https://doi.org/10.1016/S0093-934X(02)00531-X

Hutsler JJ, Galuske RAW (2003) Hemispheric asymmetries in cerebral cortical networks. Trends Neurosci 26(8):429–435. https://doi.org/10.1016/S0166-2236(03)00198-X

Jones DK, Knösche TR, Turner R (2013) White matter integrity, fiber count, and other fallacies: the do's and don'ts of diffusion MRI. NeuroImage 73(June):239–254. https://doi.org/10.1016/j.neuroimage.2012.06.081

Keller SS, Crow T, Foundas A, Amunts K, Roberts N (2009) Broca's area: nomenclature, anatomy, typology and asymmetry. Brain Lang 109(1):29–48. https://doi.org/10.1016/j.bandl.2008.11.005

Kong X-Z, Mathias CR, Guadalupe T, ENIGMA Laterality Working Group, Glahn DC, Franke B, Crivello F et al (2018) Mapping cortical brain asymmetry in 17,141 healthy individuals worldwide via the ENIGMA consortium. Proc Natl Acad Sci 115(22):E5154–E5163. https://doi.org/10.1073/pnas.1718418115

Le Guen Y, Leroy F, Auzias G, Riviere D, Grigis A, Mangin J-F, Coulon O, Dehaene-Lambertz G, Frouin V (2018) The chaotic morphology of the left superior temporal sulcus is genetically constrained. NeuroImage 174(July):297–307. https://doi.org/10.1016/j.neuroimage.2018.03.046

Lebois A (2014) Brain microstructure mapping using quantitative and diffusion MRI. PhD thesis, Université Paris Sud-Paris XI. https://tel.archives-ouvertes.fr/tel-01063198/document

Leroy F, Cai Q, Bogart SL, Dubois J, Coulon O, Monzalvo K, Fischer C et al (2015) New human-specific brain landmark: the depth asymmetry of superior temporal sulcus. Proc Natl Acad Sci USA 112(4):1208–1213. https://doi.org/10.1073/pnas.1412389112

Lopez-Barroso D, Catani M, Ripollés P, Dell'Acqua F, Rodríguez-Fornells A, de Diego-Balaguer R (2013) Word learning is mediated by the left arcuate fasciculus. Proc Natl Acad Sci 110(32):13168–13173. https://doi.org/10.1073/pnas.1301696110

Margulies DS, Ghosh SS, Goulas A, Falkiewicz M, Huntenburg JM, Langs G, Bezgin G et al (2016) Situating the default-mode network along a principal gradient of macroscale cortical organization. Proc Natl Acad Sci 113(44):12574–12579. https://doi.org/10.1073/pnas.1608282113

McGettigan C, Faulkner A, Altarelli I, Obleser J, Baverstock H, Scott SK (2012) Speech comprehension aided by multiple modalities: behavioural and neural interactions. Neuropsychologia 50(5):762–776. https://doi.org/10.1016/j.neuropsychologia.2012.01.010

Meyer L, Obleser J, Anwander A, Friederici AD (2012) Linking ordering in broca's area to storage in left temporo-parietal regions: the case of sentence processing. NeuroImage 62(3):1987–1998. https://doi.org/10.1016/j.neuroimage.2012.05.052

Mezer A, Yeatman JD, Stikov N, Kay KN, Cho N-J, Dougherty RF, Perry ML et al (2013) Quantifying the local tissue volume and composition in individual brains with magnetic resonance imaging. Nat Med 19(12):1667–1672

Mezer A, Rokem A, Berman S, Hastie T, Wandell BA (2016) Evaluating quantitative proton-density-mapping methods. Hum Brain Mapp 37(10):3623–3635. https://doi.org/10.1002/hbm.23264

Nucifora PGP, Verma R, Melhem ER, Gur RE, Gur RC (2005) Leftward asymmetry in relative fiber density of the arcuate fasciculus. NeuroReport 16(8):791–794

Pestilli F, Yeatman JD, Rokem A, Kay KN, Wandell BA (2014) Evaluation and statistical inference for living connectomes. Nat Methods 11(10):1058–1063. https://doi.org/10.1038/nmeth.3098

Poeppel D, Hickok G (2004) Towards a new functional anatomy of language. Cognition 92(1–2):1–12. https://doi.org/10.1016/j.cognition.2003.11.001

Popper K (1962) The logic of scientific discovery, revised edition. Hutchinson, Paris

Rampinini AC, Handjaras G, Leo A, Cecchetti L, Ricciardi E, Marotta G, Pietrini P (2017) Functional and spatial segregation within the inferior frontal and superior temporal cortices during listening, articulation imagery, and production of vowels. Sci Rep 7(1):17029. https://doi.org/10.1038/s41598-017-17314-0

Reese TG, Heid O, Weisskoff RM, Wedeen VJ (2003) Reduction of Eddy-current-induced distortion in diffusion MRI using a twice-refocused spin echo. Magn Reson Med 49(1):177–182. https://doi.org/10.1002/mrm.10308

Rilling JK (2014) Comparative primate neurobiology and the evolution of brain language systems. Curr Opin Neurobiol 28:10–14. https://doi.org/10.1016/j.conb.2014.04.002

Rilling JK, Glasser MF, Jbabdi S, Andersson J, Preuss TM (2012) Continuity, divergence, and the evolution of brain language pathways. Front Evol Neurosci. https://doi.org/10.3389/fnevo.2011.00011

Rogalsky C, Hickok G (2010) The role of Broca's area in sentence comprehension. J Cogn Neurosci 23(7):1664–1680. https://doi.org/10.1162/jocn.2010.21530

Schell M, Zaccarella E, Friederici AD (2017) Differential cortical contribution of syntax and semantics: an FMRI study on two-word phrasal processing. Cortex 96(Suppl C):105–120. https://doi.org/10.1016/j.cortex.2017.09.002

Schenker NM, Hopkins WD, Spocter MA, Garrison AR, Stimpson CD, Erwin JM, Hof PR, Sherwood CC (2010) Broca's area homologue in chimpanzees (*Pan troglodytes*): probabilistic mapping, asymmetry, and comparison to humans. Cereb Cortex (New York, NY) 20(3):730–742. https://doi.org/10.1093/cercor/bhp138

Setsompop K, Fan Q, Stockmann J, Bilgic B, Huang S, Cauley SF, Nummenmaa A et al (2018) High-resolution in vivo diffusion imaging of the human brain with generalized slice dithered enhanced resolution: simultaneous multislice (GSlider-SMS). Magn Reson Med 79(1):141–151. https://doi.org/10.1002/mrm.26653

Smith RE, Tournier J-D, Calamante F, Connelly A (2012) Anatomically-constrained tractography: improved diffusion MRI streamlines tractography through effective use of anatomical information. NeuroImage 62(3):1924–1938. https://doi.org/10.1016/j.neuroimage.2012.06.005

Stuber C, Morawski M, Schafer A, Labadie C, Wahnert M, Leuze C, Streicher M et al (2014) Myelin and iron concentration in the human brain: a quantitative study of MRI contrast. NeuroImage. https://doi.org/10.1016/j.neuroimage.2014.02.026

Thiebaut de Schotten M, Ffytche DH, Bizzi A, Dell'Acqua F, Allin M, Walshe M, Murray R, Williams SC, Murphy DGM, Catani M (2011) Atlasing location, asymmetry and inter-subject variability of white matter tracts in the human brain with MR diffusion tractography. NeuroImage. https://doi.org/10.1016/j.neuroimage.2010.07.055

Toga AW, Thompson PM (2003) Mapping brain asymmetry. Nat Rev Neurosci 4(1):37–48. https://doi.org/10.1038/nrn1009

Tournier J-D, Calamante F, Connelly A (2007) Robust determination of the fibre orientation distribution in diffusion MRI: non-negativity constrained super-resolved spherical deconvolution. NeuroImage 35(4):1459–1472. https://doi.org/10.1016/j.neuroimage.2007.02.016

Tournier J-D, Calamante F, Connelly A (2010) Improved probabilistic streamlines tractography by 2nd order integration over fibre orientation distributions | request PDF. In: Proc. Intl. Soc. Mag. Reson. Med, 1670. https://cds.ismrm.org/protected/10MProceedings/files/1670_4298.pdf

Tremblay P, Dick AS (2016) Broca and Wernicke are dead, or moving past the classic model of language neurobiology. Brain Lang 162:60–71. https://doi.org/10.1016/j.bandl.2016.08.004

Van Essen DC, Smith SM, Barch DM, Behrens TEJ, Yacoub E, Ugurbil K, WU-Minn HCP Consortium (2013) The WU-Minn Human Connectome Project: an overview. NeuroImage 80:62–79. https://doi.org/10.1016/j.neuroimage.2013.05.041

Vigneau M, Beaucousin V, Herve PY, Duffau H, Crivello F, Houde O, Mazoyer B, Tzourio-Mazoyer N (2006) Meta-analyzing left hemisphere language areas: phonology, semantics, and sentence processing. NeuroImage 30(4):1414–1432. https://doi.org/10.1016/j.neuroimage.2005.11.002

Vu AT, Auerbach E, Lenglet C, Moeller S, Sotiropoulos SN, Jbabdi S, Andersson J, Yacoub E, Ugurbil K (2015) High resolution whole brain diffusion imaging at 7T for the Human Connectome Project. NeuroImage 122(November):318–331. https://doi.org/10.1016/j.neuroimage.2015.08.004

Waehnert MD, Dinse J, Schäfer A, Geyer S, Bazin P-L, Turner R, Tardif CL (2016) A subject-specific framework for in vivo myeloarchitectonic analysis using high resolution quantitative MRI. NeuroImage 125:94–107. https://doi.org/10.1016/j.neuroimage.2015.10.001

Wakana S, Caprihan A, Panzenboeck MM, Fallon JH, Perry M, Gollub RL, Hua K et al (2007) Reproducibility of quantitative tractography methods applied to cerebral white matter. NeuroImage 36(3):630–644. https://doi.org/10.1016/j.neuroimage.2007.02.049

Warren JD, Scott SK, Price CJ, Griffiths TD (2006) Human brain mechanisms for the early analysis of voices. NeuroImage 31(3):1389–1397. https://doi.org/10.1016/j.neuroimage.2006.01.034

Weber K, Christiansen MH, Petersson KM, Indefrey P, Hagoort P (2016) FMRI syntactic and lexical repetition effects reveal the initial stages of learning a new language. J Neurosci 36(26):6872–6880. https://doi.org/10.1523/JNEUROSCI.3180-15.2016

Wernicke C (1874) Der aphasische Symptomencomplex: eine psychologische Studie auf anatomischer Basis. Breslau, Cohn and Weigert, Wroclaw

Wilkinson M (2013) Testing the null hypothesis: the forgotten legacy of Karl Popper? J Sports Sci 31(9):919–920. https://doi.org/10.1080/02640414.2012.753636

Yeatman JD, Dougherty RF, Myall NJ, Wandell BA, Feldman HM (2012) Tract profiles of white matter properties: automating fiber-tract quantification. PLoS One. https://doi.org/10.1371/journal.pone.0049790

Yeatman JD, Wandell BA, Mezer AA (2014) Lifespan maturation and degeneration of human brain white matter. Nat Commun. https://doi.org/10.1038/ncomms5932

Yeo BT, Thomas FM, Krienen JS, Sabuncu MR, Lashkari D, Hollinshead M, Roffman JL et al (2011) The organization of the human cerebral cortex estimated by intrinsic functional connectivity. J Neurophysiol 106(3):1125–1165. https://doi.org/10.1152/jn.00338.2011

Zilles K, Amunts K (2018) Cytoarchitectonic and receptorarchitectonic organization in Broca's region and surrounding cortex. Curr Opin Behav Sci 21:93–105. https://doi.org/10.1016/j.cobeha.2018.02.011

Zilles K, Bacha-Trams M, Palomero-Gallagher N, Amunts K, Friederici AD (2015) Common molecular basis of the sentence comprehension network revealed by neurotransmitter receptor fingerprints. Cortex 63(February):79–89. https://doi.org/10.1016/j.cortex.2014.07.007